

Short Communication

## Effect of Magnetic Field on Corrosion Behavior of X52 Pipeline Steel in Simulated Soil Solution: PART II. Influence of Direct Current Stray

Yong Yang, Wenshen Ran, Qingbao Zhang Ming Sun\*

China Special Equipment Inspection and Research Institute, Beijing 100029

\*E-mail: [39530354@qq.com](mailto:39530354@qq.com)

Received: 28 November 2021 / Accepted: 27 December 2021 / Published: 5 April 2022

Direct current interference can cause serious corrosion of oil and gas pipelines in a short time. Magnetic flux leakage (MFL) internal detection is currently the most effective and widely used nondestructive technology for detecting metal damage in oil and gas pipelines. Potentiostatic polarization, surface analysis technology and weight loss method were used to study the influence of the magnetic field generated by the magnetization of oil and gas pipelines on the corrosion behavior of the X52 pipeline steel in a Yingtan simulated soil solution. The results showed that the magnetic field increased the corrosion rate by up to 48% for samples that were potentiostatically polarized at a potential of 0.5 V; this made the corrosion products looser, but it had no obvious effect on the corrosion morphology. Through mechanism analysis, it was found that the Loren magnetic force could increase the diffusion rate of solution particles, thereby reducing the  $\text{Fe}^{2+}$  concentration at the electrode/solution interface and the thickness of the interfacial diffusion layer and eventually increasing the corrosion rate. The edge area of the defect with a geometric mutation had higher magnetic induction intensity and magnetic field gradient, and the accumulation of a higher concentration of  $\text{Fe}^{2+}$  under the action of the magnetic field gradient could to a certain extent inhibit corrosion of a local area. The conclusions of this paper indicate that the evaluation standard of stray direct current corrosion of oil and gas pipelines tested by in-line inspections on the basis of the magnetic flux leakage (MFL) principle should be improved.

**Keywords:** Magnetic field, Simulated soil solution, X52 pipeline steel, Direct current interference, Corrosion behavior

### 1. INTRODUCTION

With the rapid growth of demand for oil and gas resources because of economic and social development, the length of China's oil and gas pipelines reached  $13.5 \times 10^4$  km in 2019 [1]. Stray direct current (DC) interference caused by DC electrification facilities (such as high-voltage DC transmission systems, DC electrified railways, and rail transit) severely accelerate the corrosion of oil and gas

pipelines and cause safety hazards [2-7]. Magnetic flux leakage (MFL) internal detection technology is currently the most effective and widely used nondestructive method for detecting metal damage in oil and gas pipelines [8]. When implementing MFL detection for oil and gas pipelines, the magnetization of pipeline steel needs to be saturated with a magnetic flux of about 1.8 Tesla. The degaussing process of the magnetization of steel pipelines is affected by many factors. There is no published detailed engineering research data at present, and it has been reported that a residual magnetic field of 0.3~1.5 Tesla can last from several hours to several weeks[9]. However, it was found during maintenance that residual magnetism was still in the pipeline two years after the implementation of MFL detection, and the detection technology based on the principle of weak magnetic field could not be applied to the pipeline. The influence of a magnetic field on stray DC corrosion behavior has caused concern for pipeline transportation industry personnel.

Previous studies have shown that an applied magnetic field affects the electrochemical corrosion behavior of metals to varying degrees. Zhang [10] applied an external magnetic field with permanent magnets and found that the natural corrosion rate of X80 steel in the Shenyang meadow soil in China increased with an increase in the applied magnetic field strength and that the corrosion rate increased about 6-fold compared to the natural corrosion when the magnetic flux density was 20 mT. Hui [11] used a similar experimental method and found that an external magnetic field with a magnetic flux of 180 mT increased the corrosion rate of X60 steel by approximately 3 times in the soil of the Changsha area. Jackson [9] found that the applied magnetic field can aggravate pitting and crack defects on the surface of X70 and X80 pipeline steel samples, but Espina-Hernández [12] reported that a magnetic field can reduce pitting depth and pitting number. Stray DC corrosion of oil and gas pipelines is essentially an anodic polarization reaction of metals. Wang [13] reported that the magnetic field reduces the hydration of iron ions so that the force of the desorption is greater than the force of the adsorption on the interface, and this promotes the anodic corrosion of iron in acidic and alkaline solutions. Cai [14] believed that the Lorentz force produced magnetohydrodynamic flow, accelerating the diffusion of ferrous ions and increasing the high-potential anodic polarization current. Lu [15] reported that the magnetic field can increase the anodic polarization current of iron in dilute sulfuric acid, and this was attributed to the Loren magnetic force, which strengthens the diffusion of reactive ions and reduces the thickness of the diffusion layer and the ion concentration gradient. Sueptitz [16] found that the applied magnetic field parallel to the corrosion surface of a small sample increases the anodic polarization current of the diffusion-controlled reaction and that perpendicular to the corrosion surface decreases it; also, the magnetic field gradient force reduces the anodic polarization current in some strong magnetic field regions. It was found that the effect of the magnetic field on the stray DC corrosion is affected by many factors, and in the abovementioned anodic polarization studies, the test samples and the electrolytic solution were placed in an external vertical or parallel magnetic field, which is significantly different from the objective actual situation for a pipeline tested with MFL.

In a previous paper [17], we studied the influence that a magnetic field has on the free corrosion behavior of X52 pipeline steel in simulated Yingtan soil solution using specially designed specimens. In this paper, we optimized the experimental device and studied the influence of magnetic fields on stray DC corrosion, which is extremely harmful to oil and gas pipelines.

Using a home-designed experimental device to simulate real leakage of a magnetic field, the

influence of a magnetic field that is generated by magnetized pipelines on stray DC corrosion behavior of X52 pipeline steel samples in simulated Yingtan soil solution were studied using anode potentiostatic polarization, electrochemical impedance spectroscopy (EIS), scanning electron microscopy (SEM), energy dispersive X-ray spectroscopy (EDS), optical microscopy, and weight loss tests. The research results can be used to guide the evaluation of the hazards of stray DC corrosion of oil and gas pipelines tested with MFL and to provide a theoretical support for the formulation of relevant evaluation standards.

## 2. EXPERIMENTAL

Samples with dimensions of 10×10×6 mm were prepared from API-5L grade X52 pipeline steel, which had a chemical composition (wt %) of: C 0.20, Si 0.45, Mn 1.60, P 0.02, S 0.01, and Fe balance. To simulate the actual situation, a 10 mm-wide ring was cut from a Ø219×6 mm pipe, and 650 turns of insulated copper wire (with a copper core diameter of 0.82 mm) were wound, and a slot was cut into the ring to embed the test sample. The electrolytic cell that was used for the test was made of nylon plastic, and the lower surface was processed with a Ø7 mm circular through-hole to connect the sample. The joint surface was sealed with a silicone gasket, and the working surface was immersed horizontally in the solution. Photos of the experimental setup are showed in Figure 1. Before the experiment, the working surfaces of the samples were sequentially ground with waterproof emery papers up to 600 grit and sequentially cleaned with acetone and alcohol. The test solution that was used was a simulated Yingtan soil solution that contained [18] 0.222 g/L CaCl<sub>2</sub>, 0.936 g/L NaCl, 0.284 g/L Na<sub>2</sub>SO<sub>4</sub>, 0.394 g/L MgSO<sub>4</sub>·7H<sub>2</sub>O, 0.586 g/L KNO<sub>3</sub>, and 0.302 g/L NaHCO<sub>3</sub>. Analytical grade reagents and deionized water are used to prepare the simulation solution. NaOH and acetic acid solutions were used to adjust the pH of the solution to 4.1.

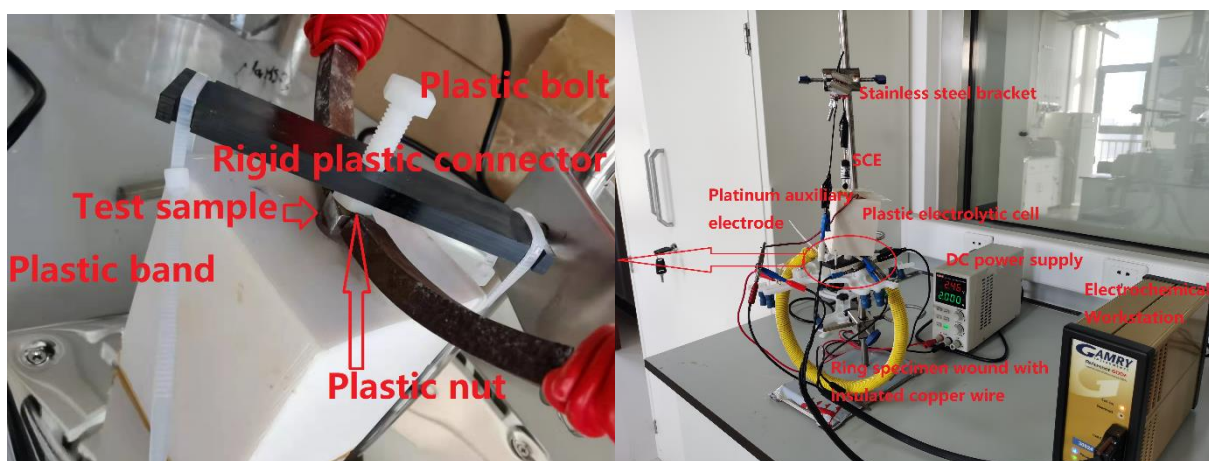


Figure 1. Photos of the experimental setup

The potentiostat was a Gamry Reference 600 Versastat device that was controlled using

Framework V7.03 software. SCE was used as the reference electrode, and a platinum plate was used as the counter electrode. The potentiodynamic curve of X52 steel in the experimental solution was measured; there was no passivation in the anodic polarization within the potential range of no more than 1.2 V, and a 0.5 V potential was selected for the anodic potentiostatic polarization to simulate DC stray current corrosion. X52 steel samples were immersed in simulated soil solution for 3 h under the following three conditions, and the EIS measurement was started after the OCP stabilized: (1) free corrosion, (2) potentiostatic polarization at a potential of 0.5 V, and (3) potentiostatic polarization at a potential of 0.5 V with magnetization. EIS measurements were carried out at OCP with a sinusoidal potential excitation of  $\pm 10$  mV in amplitude over a frequency range of 0.01-10000 Hz. The EIS results were analyzed and fitted to equivalent circuits using ZSimpWin V3.60. During the experiment, a 2A direct current was applied to the toroidal winding coil to simulate the magnetization of the sample, and the magnetic field intensity that was calculated using formula (1) was 1.9 KA/m. A Hitachi S-3500 scanning electron microscope was used to observe the corrosion products; specifically, the corrosion surface morphology was observed, and the corrosion product EDS was analyzed.

$$H = \frac{NI}{L} \quad (1)$$

where H is the magnetic field strength (A/m), N is the number of turns of the coil, I is the current value in the coil (A), and L is the length of the magnetic circuit (m), that is, the circumference of the ring. Related research [19] showed that under a magnetic field intensity of 4.5 KA/m, the magnetic flux intensity of X52 steel is not greater than 1.5T; thus, the sample in this research was in an unsaturated magnetization state.

Before and after the experiment, samples for the weight loss test were weighed using a high-precision electronic balance, and then the average corrosion rate was calculated as follows:

$$R_{\text{cor}} = 8.76 \times \Delta W / (S \times t \times \rho) \quad (2)$$

where  $\Delta W$  is the average weight-loss of the samples (g), S is the sample working surface area ( $\text{m}^2$ ), t is the experiment time (h),  $\rho$  is the density of the steel ( $\text{g}/\text{cm}^3$ ), and  $R_{\text{cor}}$  is the corrosion rate in (mm/a). All of the experiments were performed at room temperature.

### 3. RESULTS AND DISCUSSION

#### 3.1 *i-t* curves

As seen in Figure 2, the samples were in an activated corrosion state during the experiment with or without a magnetic field. At the beginning of polarization, both polarization currents increased almost linearly; then, they decreased rapidly for a short time and then increased again. The current of the non-magnetic sample had a greater decrease; the second increase was not large and did not exceed the previous value.

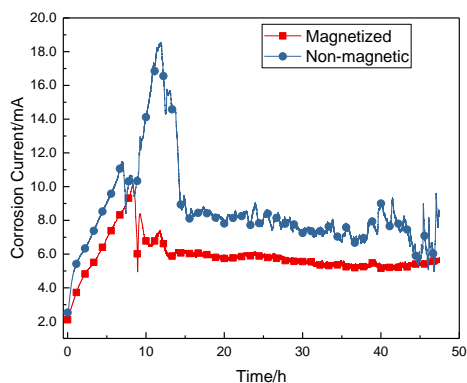


**Figure 2.** *i*-*t* curves for X52 steel in simulated Yingtan soil solution that was potentiostatically polarized at a potential of 0.5 V

The reduction in the current of the magnetized sample was relatively small, but then it greatly increased to nearly twice the previous value. After the second high point, the anode current of the two samples rapidly decreased to a certain extent and remained basically stable; however, the change in the current of the magnetized sample still remained small within a certain range. Under the same polarization potential, the polarization current of the magnetized sample was always greater than the current of the non-magnetic sample.

### 3.2 EIS

Figure 3 shows Nyquist plots of EIS data for X52 pipeline steel samples that were immersed in simulated Yingtan soil solution for 3 h under different corrosion conditions. EIS data were fitted with the equivalent circuit model  $R_s(QR_t)$ , and the fitting results are shown in Table 1. In the equivalent circuit model,  $R_s$  represents the solution resistance,  $Q$  represents the constant phase angle element of the electric double layer capacitor, and  $R_t$  represents the charge transfer resistance. The electrochemical reaction impedance ( $670 \Omega \cdot \text{cm}^2$ ) of the naturally corroded sample is the largest, the electrochemical impedance ( $169 \Omega \cdot \text{cm}^2$ ) of the anode polarized magnetized sample is the smallest, and the electrochemical impedance ( $320 \Omega \cdot \text{cm}^2$ ) of the anode polarized non-magnetic sample is in the middle. Anodic polarization prevents the formation of a protective corrosion product film on the surface of the sample, and so, the electrochemical reaction impedance is greatly reduced. Because of various magnetic field forces, a magnetic field should increase the electrochemical reaction speed during the EIS test of a sample. The increased EIS dispersion index ( $n_{dl}$ ) of the anode polarized sample indicates that the anodic polarization causes the surface state of the sample to be more uniform so that the corrosion current density distribution during the EIS test is more uniform.

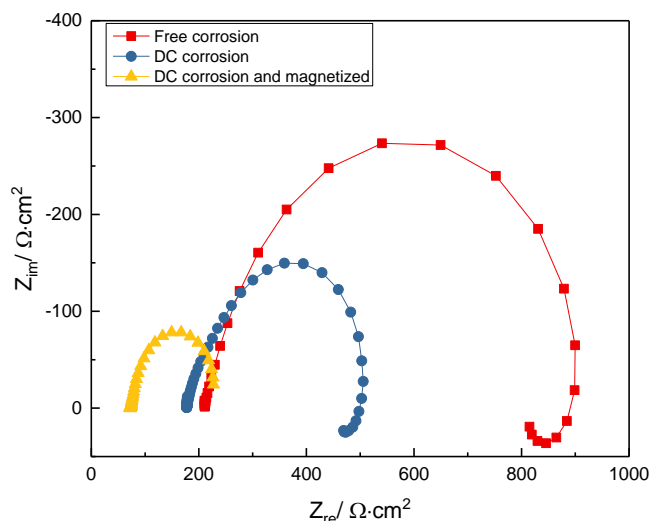


**Figure 3.** Nyquist plots of EIS of X52 pipeline steel samples that were immersed in simulated Yingtan soil solution for 3h under different corrosion conditions

**Table 1.** Equivalent circuit fitting for the EIS data of X52 pipeline steel samples

Corrosion conditions	$R_s/\Omega\cdot\text{cm}^2$	$Y_{dl}/(\text{Ssn}/\text{cm}^2)$	$n_{dl}$	$R_t/\Omega\cdot\text{cm}^2$
Free corrosion	213	$1.370\times 10^{-4}$	0.8538	670
DC corrosion	180	$1.305\times 10^{-3}$	0.9192	320
DC corrosion and magnetized	73	$1.542\times 10^{-2}$	0.9262	169

### 3.3 Corrosion rate

As seen from Figure 4, the corrosion rate of the sample that was subjected to a 0.5 V potential direct current is much greater than the rate of natural corrosion (0.19 mm/a).

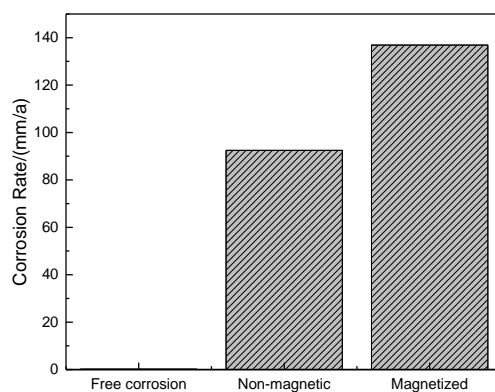


**Figure 4.** Corrosion rates of X52 steel samples in simulated Yingtan soil solution: free corrosion for 96 h and potentiostatically polarized at a potential of 0.5 V for 48 h with and without a magnetic field

Also, the corrosion rate of the magnetized sample under a magnetic field strength of 1.9 KA/m (136.88 mm/a) is significantly higher than the corrosion rate of non-magnetic samples (92.48 mm/a), and the rate increases up to 48%. The corrosion rates of the magnetized and non-magnetic samples were calculated according to Faraday's law and from polarization current (Figure 2); the values were 128.72 and 87.58 mm/a, respectively. The values obtained by Faraday's law were little smaller, and this may be caused by test error and sample handling.

### 3.4 Corrosion products

Figure 5 shows the morphology of the lower layer of corrosion products after the loose corrosion products were cleaned from the surface via ultrasonic waves in absolute ethanol for the same length of time. The corrosion products of the non-magnetic samples were relatively dense, but they were thin and have many small cracks. Also, the corrosion products of the magnetized samples were significantly looser, but relatively thicker; these were similar to the corrosion results of X80 pipeline steel affected by a magnetic field [10]. The looser corrosion products of the magnetized samples may be related to the force of the magnetic field when the corrosion product particles are accumulated.

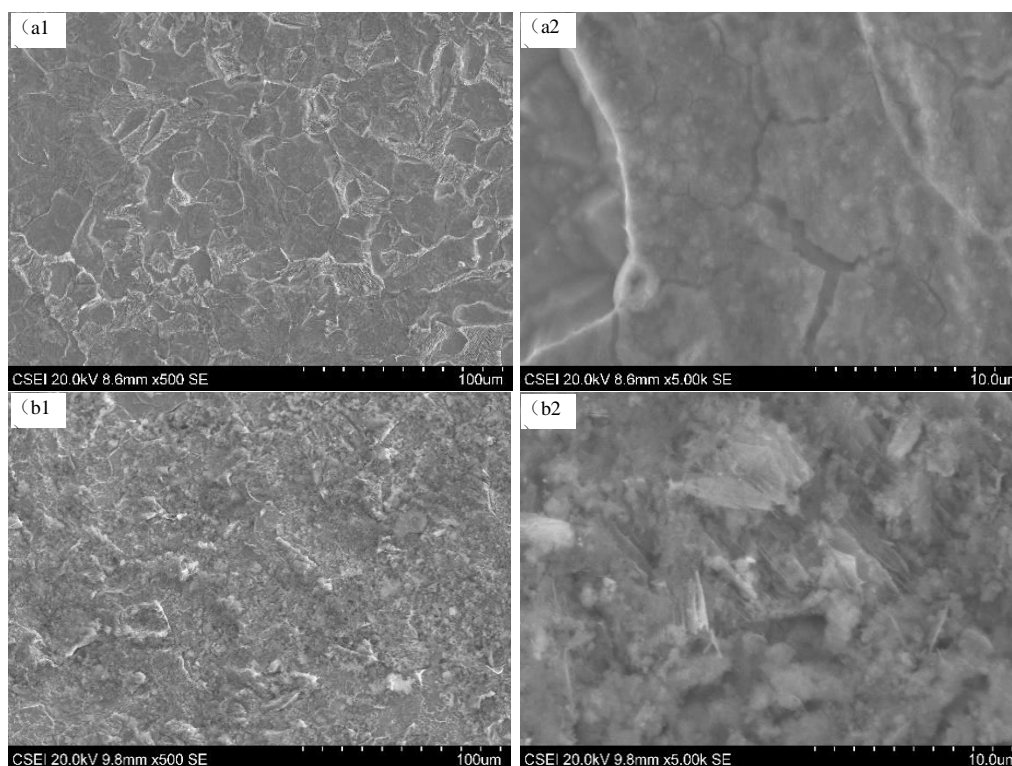


**Figure 5.** Morphologies of corrosion product of X52 steel samples in simulated Yingtan soil solution potentiostatically polarized at a potential of 0.5 V for 48 h: (a1,a2) non-magnetic and (b1,b2) magnetized

As seen from Figure 6, the corrosion products are mainly composed of iron and oxygen and contain small amounts of carbon and chlorine. The oxygen content in the corrosion products of the

magnetized samples was significantly higher than that of the non-magnetic samples. It may be that magnetohydrodynamics increased the transmission of oxygen to the reaction interface and increased the oxygen content.

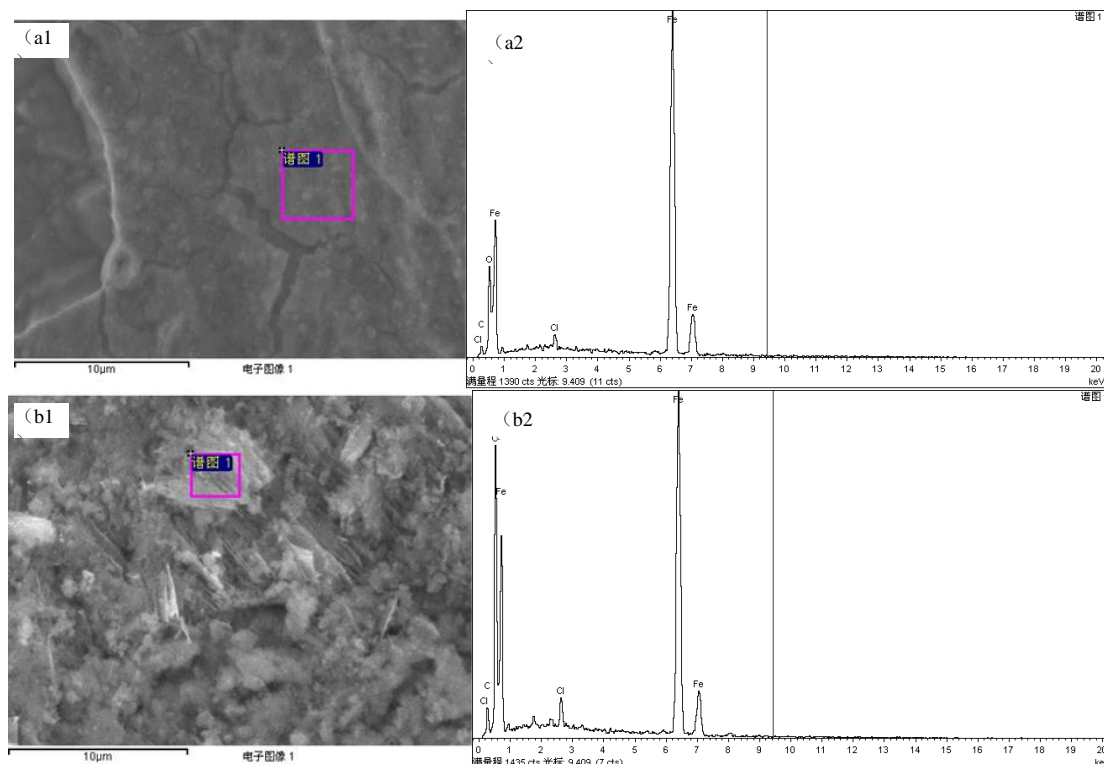


**Figure 6.** EDS analysis of the corrosion product of X52 steel samples in simulated Yingtan soil solution potentiostatically polarized at a potential of 0.5 V for 48 h: (a1,a2) non-magnetic and (b1,b2) magnetized

### 3.5 Corrosion morphologies

As shown in Figure 7, the macroscopic corrosion morphologies of non-magnetic and magnetized X52 steel samples in simulated Yingtan soil solution that were potentiostatically polarized at a potential of 0.5 V for 48 h were similar. Specifically, there was a regular circular corrosion pit with a flat bottom and a spherical arc in the vertical section. The depth of the corrosion pit of the magnetized sample (1.47 mm) was greater than that of the non-magnetic sample (0.89); however, the diameter of the corrosion pit of the non-magnetic sample was slightly larger than that of the magnetized sample, and its vertical arc was steeper.

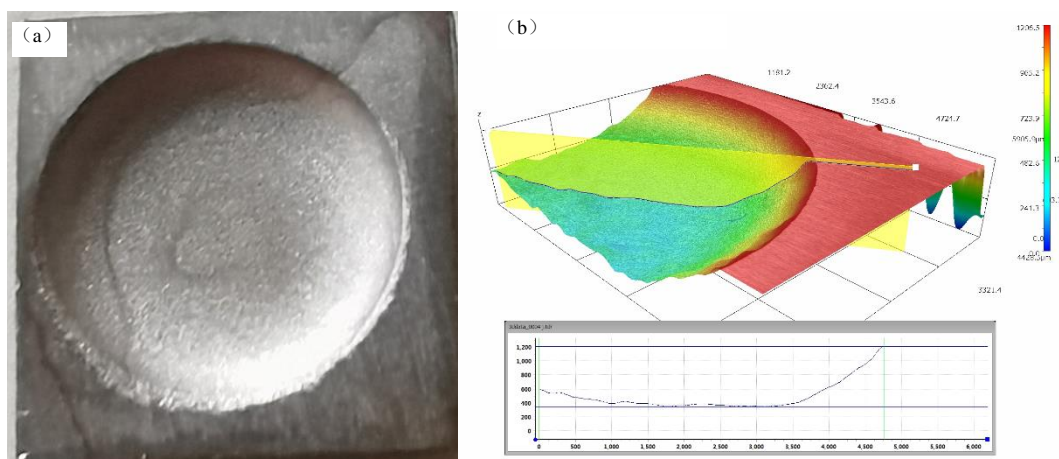


**Figure 7.** Macroscopic corrosion morphology of X52 steel samples in simulated Yingtan soil solution potentiostatically polarized at a potential of 0.5 V for 48 h: (a) optical photo and (b) 3-dimensional composite image

Figure 8 shows the microscopic morphologies of the bottom of corrosion pits of non-magnetic and magnetized X52 pipeline steel in simulated Yingtan soil liquid with 0.5 V anodic polarization for 48 h. The corrosion with or without magnetization was relatively smooth and uniform corrosion, and there were no obvious differences in the microscopic corrosion morphologies.

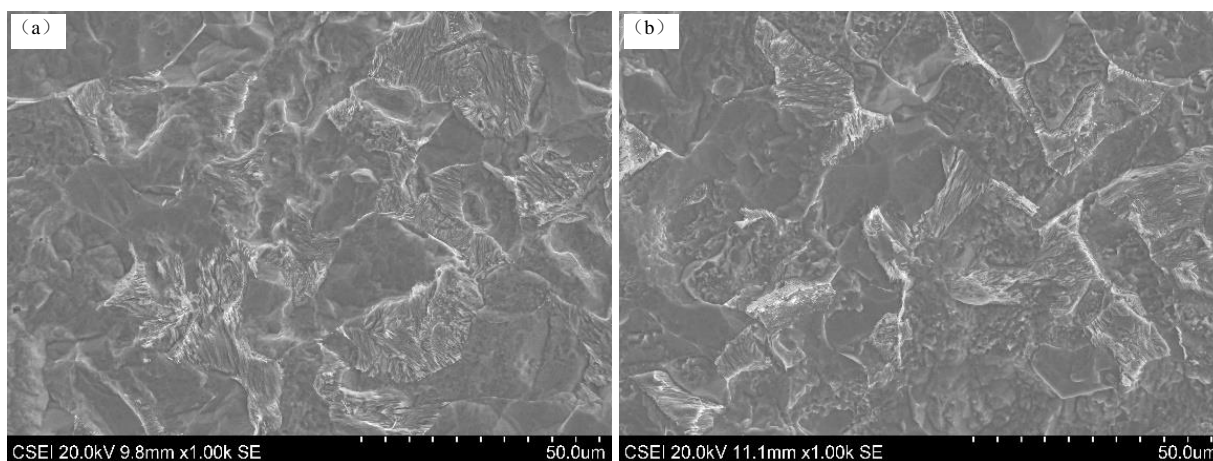


**Figure 8.** Microscopic morphologies of the corrosion pit bottom of X52 steel samples in simulated Yingtan soil solution potentiostatically polarized at a potential of 0.5 V for 48 h: (a) non-magnetic and (b) magnetized

Figure 9 shows the microscopic morphology of the corrosion pit edge of non-magnetic and magnetized X52 pipeline steel in simulated Yingtan soil solution with 0.5 V anode polarization for 48 h. The edge of the corrosion pit of the non-magnetic sample is more severely corroded than that of the

magnetized sample. This may be related to the greater magnetic field gradient force at the edge of the corrosion pit.

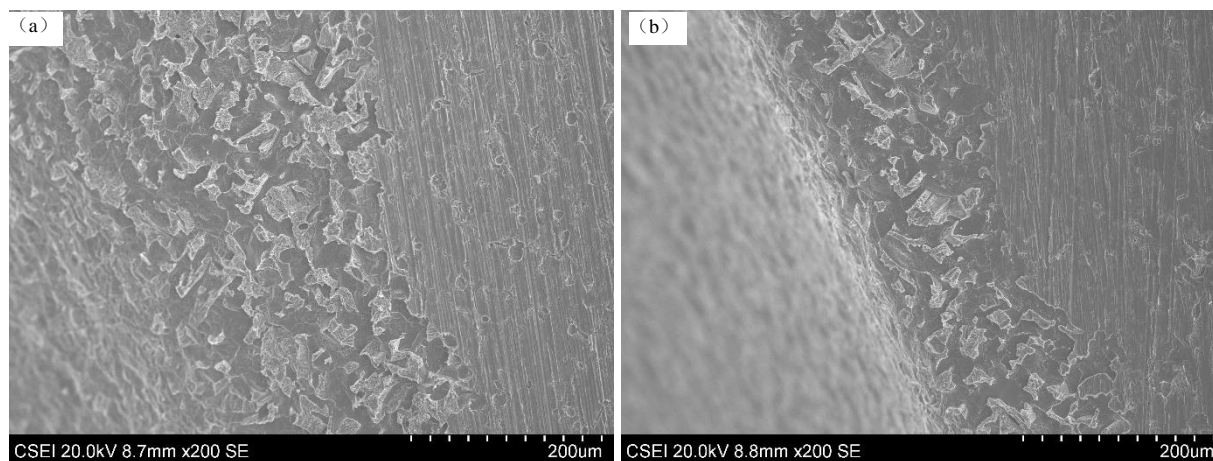


**Figure 9.** Microscopic morphologies of the corrosion pit edge of X52 steel samples in simulated Yingtan soil solution potentiostatically polarized at a potential of 0.5 V for 48 h: (a) non-magnetic and (b) magnetized

#### 4. DISCUSSION

The magnitude of the magnetic flux intensity of a magnetic field that acts on the corrosion interface is an important factor that affects the electrochemical reaction. Compared to the case of a direct application of a magnetic field that was perpendicular or parallel to the working surface of an electrode in most studies, the magnitude of the leakage magnetic field that acts on the electrochemical reaction in this study depends on the strength of the magnetic field loaded in the ring and the surface roughness of the sample (equivalent to numerous tiny defects) or the size and shape of the defects. A schematic diagram of the leakage magnetic field that formed around a single defect on the surface of the sample is shown in Figure 10. Different areas of the defect have different magnetic flux strengths and directions.

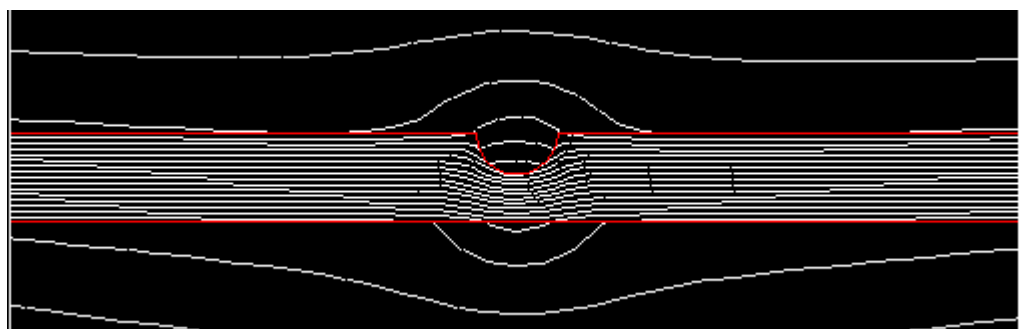


**Figure 10.** Schematic diagram of distribution of the magnetic flux intensity on the surface of the sample

Related studies showed that the magnetic field has no effect on the electron transfer process of

an electrochemical reaction, but it has an important effect on the diffusion process of the reaction medium [20-23]. The magnetic field forces that have an effect on the mass transfer process of the solution mainly include the Loren magnetic force [24], magnetic field gradient force [25], and paramagnetic gradient force [21]; the formation conditions and strength of the influencing factors are different. Among these, the paramagnetic gradient force originates from the magnetization of paramagnetic particles; this is consistent with the direction of the ion concentration gradient. Specifically, it is the opposite of the ion diffusion driving force and is much smaller than the ion diffusion driving force [21]. Also, its effect is negligible in this study.

As shown in formula (3), a Loren magnetic force ( $F_L$ ) is produced when charged ions move in a magnetic field, where  $J$  is the energy density of the charged ions and  $B$  is the magnetic flux intensity.

$$F_L = J \times B \quad (3)$$

In this study, the continuous anodic current that flows from the reaction interface to the solution body cuts the magnetic lines of the force at the surface defects of the sample, as shown in Figure 10. Also, the generated Loren magnetic force drives the rotating motion of the nearby corrosive medium to increase the diffusion rate of the reaction material; this thereby reduces the iron ion concentration at the reaction surface and reduces the thickness of the interface diffusion [15]. As shown in Figure 2, the polarization current of the two samples increased almost linearly at the beginning of the polarization, and this is because of an increase in the reaction area as the corrosion progresses and a decrease in the solution impedance as a result of the increase in the  $Fe^{2+}$  concentration near the corrosion reaction interface [26]. The greater polarization current of the magnetized sample can be attributed to the Loren magnetic force. After the polarization current of the non-magnetic sample reaches a maximum, it decreases to a certain value because of the corrosion products. In this state, ion diffusion and the electrode reaction rate reach equilibrium and remain stable. The anodic current of the magnetized sample continued to increase to about twice that of the non-magnetic sample and then rapidly decreased. It should be that before the depth of the corrosion pit reached a certain critical value, the corrosion products in the corrosion pit were transferred out of the corrosion pit by the magnetohydrodynamic force. Thus, the corrosion products were unable to provide protection for the metal, but when the depth of the corrosion pit reached the critical value, the magnetohydrodynamic force could no longer overcome the gravitational action of the corrosion product. Then, the corrosion product precipitated and started to inhibit the polarization current; this thereby reduced the polarization current value and caused it to fluctuate within a limited range. The polarization current of the magnetized sample is always greater than that of the non-magnetic sample, and thus, the magnetized sample will eventually have a greater corrosion rate.

In a nonuniform magnetic field, the magnetic field gradient force ( $F_B$ ) as shown in formula (4) causes paramagnetic ions in a non-uniform magnetic field to move to the high magnetic induction intensity region and the diamagnetic ions to move to the low magnetic induction intensity region.

$$F_B = \frac{\chi_m c B \vec{\nabla} B}{\mu_0} \quad (4)$$

where  $\chi_m$  is the magnetic susceptibility per unit mass,  $c$  is the ion concentration,  $\mu_0$  is the absolute magnetic permeability, and  $\vec{\nabla} B$  is the magnetic gradient.

In this study, the main anodic reaction is the oxidation of Fe to  $\text{Fe}^{2+}$ , and the paramagnetic ions  $\text{Fe}^{2+}$  accumulate in the high magnetic induction area under the action of  $F_B$ . As shown in Figure 8, for a magnetized pipeline steel pipeline, the defect edge area with a sudden change in geometry has a higher magnetic flux intensity and magnetic field gradient. Therefore, under the action of  $F_B$ , a higher concentration of  $\text{Fe}^{2+}$  accumulates and inhibits corrosion at the edge. Thus, the surface size of the corrosion pit of the magnetized sample is slightly smaller than that of the non-magnetic sample, and the vertical section slope is larger. Related studies also showed that under the action of  $F_B$ , an applied magnetic field in the direction horizontal to the corrosion surface of the sample inhibits the edge corrosion in the direction of the magnetic field of the sample [15,27], and the magnetic field that was perpendicular to the corrosion surface of the sample can reduce the edge corrosion of the entire circle of the cylindrical sample [25].

## 5. CONCLUSIONS

(1) A magnetic field can promote stray direct current corrosion of X52 pipeline steel, and the corrosion rate at a 0.5 V potential increases by 48%.

(2) The magnetic field causes the stray direct current corrosion products of X52 pipeline steel to be looser, but it does not significantly change its uniform corrosion morphology.

(3) The acceleration of the Loren magnetic force on the diffusion of charged particles in the corrosion solution increases the corrosivity of the stray direct current at the same potential, but the magnetic field gradient force inhibits the corrosion in the high magnetic induction area to a certain extent.

## ACKNOWLEDGEMENTS

This research was supported by the Science and Technology Plan Projects of State Administration for Market Regulation (2019MK136), CSEI Research Program (2019-Youth-03).

## References

1. Z.W. Nie, J. Huang, Y.Z. Yu, Y.J. Wang, C. Shan. *Oil Gas Storage Transp.*, 39(01)(2020)16.
2. J.F. Yu, M. Zhang. *Mater Prot*, 48(09)(2015)14.
3. C. Yang, G. Cui, Z.L. Li, C.B. Zhang. *Mater Prot*, 49(10)(2016)18.
4. J. Hao, Y. Shuo. *Constr. Buld. Mater.* 272 (2021)121646.
5. R.Z. Qin, Y.X. Du, M.X. Lu, L. Ou, H.M. Sun. *Acta Metall Sin*, 54(06)(2018)886.
6. Y. Guo, J.F. Ding, X.Y. Li, J.R. Li. *Int. J. Electrochem. Sci.*, 16 (2021) 210547.
7. X. Yuan, Y.X. Du, Y. Liang, R.Z. Qin. *Chin J Eng*, 43(11)(2021)1560.
8. L.J. Yang, H. Geng, S.W. Gao. *Chin. J. Sci. Instrum.*, 37(08)(2016)1736.
9. J.E Jackson., A.N. Lasseigne-Jackson, F.J. Sanchez, L.David, B.Mishra. The Influence of Magnetization on Corrosion in Pipeline Steels// 6th International Pipeline Conference. Alberta, Canada, 2006.
10. K.N. Zhang, M. Wu, F. Xie, D. Wang, Y.X. San. *J. Chin. Soc. Corros.Prot.*, 37(02)(2017)148.
11. H.J. Hui, Q.S. Dai, K. Chen, Z.T. Jiang, W. Cui, Y.F. Li. *Corros. Prot.*, 40(07)(2019)474.
12. J.H. Espina-Hernández, F. Caleyó, V. Venegas, J.M. Hallen. *Corros. Sci.*, 53(2011)3100.

13. C. Wang, J.M. Chen. *J. Chin. Soc. Corros.Prot.*, 14(02)(1994)123.
14. S.W. Cai, F. Ning, Y.J. Tang, K. Zhang, T.M. Cui. *Corros. Prot.*, 41(08)(2020)1.
15. Z.P. Lu, D.L. Huang, W. Yang, J. Congleton. *Corros. Sci.*, 45(2003)2233.
16. R. Sueptitz, J. Koza, M. Uhlemann, A. Gebert, L. Schultz. *Electrochim. Acta*, 54(2009):2229.
17. Y. Yang, Y.L. Luo, M. Sun, J.Q. Wang. *Int. J. Electrochem. Sci.*, 16(2021) Article Number: 211010.
18. Y. Yang, M. Sun, Y.L. Luo, W.G. Zeng, R.Y. He. *Int. J. Electrochem. Sci.*, 16(2021) 150927.
19. R. Grossinger, F. Keplinger, N. Mehmood, H. Espina-Hernandez. *IEEE Trans. Magn.*, 44(2008)3277.
20. R. Burrows, A. Baron-wiechec, C. Harrington, S. Moore, D. Chaney, T.L. Martin, J. Likonen, R. Springell, E. Surrey. *Fusion Eng Des*, 136(2018)1000.
21. G. Hinds, J.M.D. Coey, M.E.G. Lyons. *Electrochem. Commun.*, 3(2001)215.
22. S.B. Liu, Y. Shao, C.Q. Yan, B.Y. Yuan, L. Li, C.WANG. *Corros Sci*, 169(2020)108614.
23. O. Devos, O. Aaboubi, J. Chopart, A. Olivier. *J. Phys. Chem. A*, 104(2000)1544.
24. L.M.A. Monzon, J.M.D. Coey. *Electrochem. Commun.*, 42(2014)38.
25. R. Sueptitz, K. Tschulik, M. Uhlemann, J. Eckert, A. Gebert. *Mater corros*, 65(2014)803.
26. X.J. Li, M. Zhang, B.Y. Yuan, L. Li, C. Wang. *Electrochim. Acta*, 222(2016)619.
27. H.J. Li, Q. Xiong, Z.P. Lu, J.J. Chen, Q. Xiao, X.K. Ru, S.C. Lin, J.R. Ma, Z. Chen. *Corros sci*, 129(2017)179.

© 2022 The Authors. Published by ESG ([www.electrochemsci.org](http://www.electrochemsci.org)). This article is an open access article distributed under the terms and conditions of the Creative Commons Attribution license (<http://creativecommons.org/licenses/by/4.0/>).